



Published in final edited form as:

*Proc SPIE Int Soc Opt Eng.* 2024 February ; 12926: . doi:10.1117/12.3006901.

## Learning-based Free-Water Correction using Single-shell Diffusion MRI

Tianyuan Yao<sup>a</sup>, Derek B. Archer<sup>b</sup>, Praitayini Kanakaraj<sup>a</sup>, Nancy Newlin<sup>a</sup>, Shunxing Bao<sup>c</sup>, Daniel Moyer<sup>a</sup>, Kurt Schilling<sup>d</sup>, Bennett A. Landman<sup>a,b,c,d</sup>, Yuankai Huo<sup>a,d</sup>

<sup>a</sup>Department of Computer Science, Vanderbilt University, Nashville, TN, USA

<sup>b</sup>Department of Neurology, Vanderbilt University Medical Center, Nashville, TN, USA

<sup>c</sup>Department of Electrical and Computer Engineering, Vanderbilt University, Nashville, TN, USA

<sup>d</sup>Department of Biomedical Engineering, Vanderbilt University, Nashville, TN, USA

### Abstract

Diffusion magnetic resonance imaging (dMRI) offers the ability to assess subvoxel brain microstructure through the extraction of biomarkers like fractional anisotropy, as well as to unveil brain connectivity by reconstructing white matter fiber trajectories. However, accurate analysis becomes challenging at the interface between cerebrospinal fluid and white matter, where the MRI signal originates from both the cerebrospinal fluid and the white matter partial volume. The presence of free water partial volume effects introduces a substantial bias in estimating diffusion properties, thereby limiting the clinical utility of DWI. Moreover, current mathematical models often lack applicability to single-shell acquisitions commonly encountered in clinical settings. Without appropriate regularization, direct model fitting becomes impractical. We propose a novel voxel-based deep learning method for mapping and correcting free-water partial volume contamination in DWI to address these limitations. This approach leverages data-driven techniques to reliably infer plausible free-water volumes across different diffusion MRI acquisition schemes, including single-shell acquisitions. Our evaluation demonstrates that the introduced methodology consistently produces more consistent and plausible results than previous approaches. By effectively mitigating the impact of free water partial volume effects, our approach enhances the accuracy and reliability of DWI analysis for single-shell dMRI, thereby expanding its applications in assessing brain microstructure and connectivity.

### Keywords

Diffusion MRI; Free water elimination; Deep learning; Reproducibility

## 1. INTRODUCTION

Diffusion magnetic resonance imaging (dMRI) is a noninvasive biomedical imaging technique to provide unique in vivo microstructural information, especially for the study of white matter structure and brain connectivity.<sup>1-3</sup> With in the context of diffusion tensor model (DTI), an application of dMRI, dMRI is used clinically for surgical planning.<sup>4</sup> DTI is usually used to quantify the three-dimensional movement of water with the assumption

that simple Gaussian diffusion is a good descriptor of the water diffusion within a voxel.<sup>5</sup> Meanwhile, DTI yields quantitative estimates of the brain,<sup>6</sup> such as fractional anisotropy (FA) which provides an indication of white matter coherence. The principal eigenvector of the diffusion tensors provides the orientation of the white matter bundles; the mean diffusivity, which provides a contrast mechanism for identifying areas with increased bulk diffusivity that may represent an increase in tissue water content. DTI indices have proven significant value in clinical evaluation and brain research, including the unique ability to delineate neuronal fibers via tractography.<sup>7</sup>

The single-tensor DTI model is limited to assuming a single tissue compartment per voxel, thus generating biased DTI metrics in voxels consisting of a mixture of white matter and freely moving extracellular water molecules.<sup>8</sup> Free water is defined as water molecules that do not experience flow and nor restricted by their surroundings. In the human brain, cerebrospinal fluid (CSF) confined to the ventricles and around the brain parenchyma as well as in lesion edema is considered free water. In dMRI, signals from free water in the CSF can ‘contaminate’ the image. The obtained MRI signal originates from both the CSF and as well as from the white matter partial, leading to potential misinterpretations.<sup>9</sup> Diffusion metrics are typically biased by Cerebrospinal fluid (CSF) contamination.<sup>8</sup> Diffusion tractography can be strongly influenced by these free water partial volume effects. This is especially crucial when studying neurodegenerative diseases such as Alzheimer’s, Multiple Sclerosis, Parkinsonism, and Schizophrenia, where subtle changes in water diffusion can be indicative of the disease’s progression.<sup>10</sup>

The Free Water Elimination (FWE) model, as proposed by Pasternak et al.,<sup>6</sup> aims to mitigate the adverse impact of CSF partial volume effects on diffusion measurements.<sup>7</sup> The initial model requires multiple b-values to distinguish the tissue types on the sub-voxel level.<sup>11</sup> More recent implementations were able to delineate fast diffusing components using single-shell data with the help of a-priori local spatial information.<sup>10</sup> Nonetheless, this traditional methodology becomes ill-posed in the absence of multi-shell constraints and certain underlying assumptions. Although the FWE model can be resolved with multiple b-value measurements,<sup>12</sup> a limited number of studies have ventured into employing these protocols for DTI. Surprisingly, none have embarked on a comprehensive evaluation of the precision in FWE fitting.

Since state-of-the-art mathematical models are often inapplicable to clinical data. Firstly, they rely on multi-shell data, which is often unavailable in clinical settings.<sup>4</sup> Second, they demand a substantial amount of computing power and take more time than what is feasible when working with patients. Furthermore, in the case of single-shell acquisitions, which are common in clinical settings, a direct model fit is not feasible. Instead, some sort of regularization needs to be introduced. This is possible via spatial regularization,<sup>6,10,13</sup> or via deep learning as in.<sup>8</sup>

In this study, we propose a novel voxel-based deep learning method<sup>14</sup> for mapping and correcting free-water partial volume contamination in DWI to address these limitations. As compared with the deep learning state-of-the-art (SOTA) method, the proposed deep learning framework can be fed with data simultaneously across a range of acquisition

settings, while targeting the free water fractions generated from Human Connectome Project (HCP) young adults dataset<sup>3,15</sup> (the acquisitions had b-values of 1000, 2000, 3000  $s/mm^2$  with 90 gradient directions on each shell.) With the combination of dynamic head and spherical convolution, this approach leverages data-driven techniques to reliably infer plausible freewater volumes across different diffusion MRI acquisition schemes, including single-shell acquisitions.

## 2. METHOD

### 2.1 Preliminaries

Traditional approaches for free water elimination predominantly rely on multi-shell diffusion MRI data, which are acquired at multiple b-values. This requirement is necessitated by the inherent differences in the diffusion behavior of water molecules in free water and brain tissue across various b-values, which these methods exploit to segregate and subtract the free water signal accurately.

In dMRI, the measured signal is the contribution of CSF and tissue (parenchyma) components where the relative signal contribution of the fast diffusing component is described by  $f$ . The free water elimination signal model is described by:

$$S = f \cdot S_{tissue} + (1 - f) \cdot S_{CSF} \quad (1)$$

which can be further shown as:

$$S = S_0[(1 - f)exp(-bg_i^T D_{tissue} g_i) + f exp(-bD_{iso})] \quad (2)$$

where the  $D_{iso}$  is the free water diffusivity and  $D_{tissue}$  is the tissue diffusion tensor. Since  $D_{tissue} < D_{iso}$ , measurements at different echo-time yield distinct contributions of tissue and free water. Thus, disentangling the volume fractions requires measurements of at least two different echo times.<sup>16</sup> Eq.2 is ill-posed when utilizing single-shell diffusion MRI data, where diffusion-sensitizing gradients are applied at a singular b-value, we will have infinite ( $f, D_{tissue}$ ) solution pairs, these standard techniques become inapplicable due to the absence of comparative signals across differing b-values.

Several works use deep learning to learn the free water (FW) fraction from single shell data.<sup>8,17</sup> However, traditional deep learning frameworks are not generalizable to new acquisition schemes.<sup>18</sup> This complicates applying a deep learning (DL) model to data acquired in different acquisition settings. Our model aims to train a DL framework that can be adapted to a multiple combination of available multi-shell dMRI sequences and single-shell sequences. To serve this motivation, we employ a dynamic head (DH) design to handle the multi-shell problem on the three most common b-values: 1000, 2000, and 3000  $s/mm^2$ . Additionally, to tackle the problem of varying gradient directions on each shell, we employ spherical CNNs while comparing with the strategy of first performing modeling

(spherical harmonics, SHORE, e.g.) and then feeding the DWI representation into an FCN. In this study, we employ free water fraction estimation as our chosen task to perform assessments on both conventional/mathematical models and other deep learning frameworks.

## 2.2 Dynamic head

In our model, a single set of model parameters is learned to handle all permutations of a different number of shells with the most commonly known b-values. The dynamic head inherits the training scheme of the multi-modality deep learning framework.<sup>19</sup> We devise a dynamic head to adaptively generate model parameters conditioned on the availability of input shells. We use a binary code where 0/1 represents the absence/presence of each shell. To mitigate the large input variation caused by artificially zero-ed channels, we use the dynamic head to generate the parameters for the first convolutional layer. A shared network is trained using the input data with different shell configurations during training.

## 2.3 Spherical convolution

Goodwin-Allcock et al. have shown spherical CNNs represent a compelling alternative that is robust to new gradient schemes as well as offering rotational equivariance.<sup>18</sup> Spherical deep learning applies convolutions between a spherical signal and learnable spherical filters, with rotation-valued output features. In Spherical CNNs, the gradient scheme is explicitly considered in the input, enabling them to better handle variations in the gradient scheme that can occur between different acquisition protocols or imaging sites. Unlike a Fully Connected Network (FCN), the input length depends on the number of neurons in the first layer. Additionally, Spherical CNNs can better handle training data distribution, as they are naturally suited to working with data on a sphere. Overall, these benefits of spherical convolution can lead to improved accuracy and robustness in the analysis of diffusion MRI signals. We used an architecture known as the hybrid spherical CNN as described in .<sup>20</sup> After the rotational invariant features are extracted, They are concatenated and fed into fully connected layers which perform the final estimation of  $f_{tissue}$ .

# 3. EXPERIMENTS

## 3.1 Data

We have chosen DW-MRI from the Human Connectome Project - Young Adult (HCP-ya) dataset,<sup>3,15</sup> 220 subjects were used. The acquisitions had b-values of 1000, 2000, 3000  $s/mm^2$  with 90 gradient directions on each shell. A T1 volume of the same subject was used for WM segmentation using SLANT.<sup>21</sup> All HCP-ya dMRIs were distortion corrected with top-up and eddy.<sup>22</sup> 200 subjects are used as training data while 10 subjects were used as evaluation and 10 subjects as testing data. To simulate different shell configurations, we reorganized the data from subjects in HCP and simulated two shells and single shell data ( $b_0$  shells are included).

In medical imaging, there are instances where a true gold standard does not exist, or it might be impractical to use. In such cases, a secondary standard, often termed a "silver standard," is employed. The silver standard might not possess the definitive accuracy of a gold standard but is still accepted as a reliable reference point. In our scenario, a conventional state-of-the-

art (SOTA) method applied on multi-shell dMRI data with diffusion gradients as much as possible serves as the silver standard. This means while it might not be the absolute best representation of the true free water fractions, it is still a reliable and accepted reference. The free water fractions are generated using the Free Water Elimination model from .<sup>6</sup> The free water DTI implementation detail was published in.<sup>7,23</sup> The tissue fraction of the non-linear least square solution on three shells' data is regarded as the silver standard in our study. We employed the HCP 1000  $s/mm^2$  shell with 6  $b_0$  volume as the testing data from subjects in the testing cohort. Our deep learning-based model, therefore, aims to bridge the gap between single-shell data and this silver standard, effectively learning to emulate a more complex method from simpler data inputs.

## 3.2 Baseline

**3.2.1 Model-based methods**—The method of Free Water Elimination from Pasternak et al.<sup>6</sup> was implemented as the baseline for the conventional FWE model. When dealing with single shell data, spatially regularized gradient descent (RGD) algorithms<sup>10</sup> applied constraints that are imposed via the time evolution of a gradient flow on a Riemannian manifold<sup>13</sup> to get a unique solution.

**3.2.2 Deep learning methods**—The ANN proposed by Molina-Romero et al.<sup>8</sup> is performed as a deep learning-based method to extract the free water fraction. We followed their settings where initializing a 4-layer FCN (two hidden layers with  $N_b/2$  and  $N_b/4$  respectively). In our case,  $N_b$  is 96. The input size is 96 and one single output unit yields the estimate of free water fractions. We trained the ANN architectures with the training Cohort. We chose the best-performing ANNs on the validation cohort and compared them against the Pasternak's with the RGD method.

Additionally, the shore basis function<sup>24–26</sup> has been shown to capture the representation of multi-shell dMRI with minimal representation error and ensure the same when modeling single-shell dMRI. Thus, we utilize the shore representation as an additional baseline to assess the representation extracted from the spherical convolution network. We used 6<sup>th</sup> order and regularization constants:  $1e-8$ . The scaling factor is carefully calculated by  $\zeta$  defined in units of  $mm^{-2}$  as  $\zeta = 1/8\pi^2\tau MD$  is calculated based on the mean diffusivity (MD) obtained from the data. We also applied a 4-layer FCN to fit the FW fraction. The input size is 50 (SHORE estimates 50 coefficients at 6<sup>th</sup>) and the sizes of the hidden layer are 100, and 50 respectively.

## 4. RESULTS

Both our proposed method and the baselines showed similar performance (a boost of FA) as shown in the histogram of Fig. 3. The RMSE with generated free water fractions and the silver standard is calculated and shown in Table. 1. From the table, the deep learning methods outperformed other methods on single-shell data on both RMSE of the prediction error of  $f_{tissue}$  and the average FA on ROI patches, a visualization of the error with the silver standard is shown in the right panel of Fig. 3. Our proposed framework has also reached an average FA of 0.508 on a selected ROI as compared with 0.517 on the silver standard.

CSF contribution was removed from all the MD maps as shown in the left panel of Fig. 4. However, from the histogram of the right panel of Fig. 4, both ANNs and the Pasternak et al. w. RGD method suffered from over-regularization of MD. Our proposed method has the closest distribution with the MD of the silver standard.

From the above results, our proposed method kept the anatomical integrity of the FA, MD. We observed the CSF correction in the enlargement of the corpus callosum and fornix, and a general increment of FA in white matter, compared to the silver standard.

## 5. CONCLUSION

The study shows the deep-learning method trained with HCP data is capable of estimating the tissue volume fraction from the measured single-shell diffusion signal. The correction on single-shell diffusion MRI of our proposed framework outperforms the conventional method: Pasternak et al. with regularized gradient descent. With the application of our method to remove CSF contamination, we proved that tissue volume in single-shell data can be estimated by our proposed method. This approach leverages data-driven techniques to reliably infer plausible free-water volumes across different diffusion MRI acquisition schemes.

## ACKNOWLEDGMENTS

This work was supported by the National Institutes of Health under award numbers R01EB017230, 1R01DK135597-01, T32EB001628, and 5T32GM007347, and in part by the National Center for Research Resources and Grant UL1 RR024975-01. This study was also supported by the National Science Foundation (1452485, 1660816, and 1750213). The Vanderbilt Institute for Clinical and Translational Research (VICTR) is funded by the National Center for Advancing Translational Sciences (NCATS) Clinical Translational Science Award (CTSA) Program, Award Number 5UL1TR002243-03. The content is solely the responsibility of the authors and does not necessarily represent the official views of the NIH or NSF.

## REFERENCES

- [1]. Basser PJ, Mattiello J, and LeBihan D, "Estimation of the effective self-diffusion tensor from the nmr spin echo," *Journal of Magnetic Resonance, Series B* 103(3), 247–254 (1994). [PubMed: 8019776]
- [2]. Van Essen DC, Ugurbil K, Auerbach E, Barch D, Behrens TE, Bucholz R, Chang A, Chen L, Corbetta M, Curtiss SW, et al. , "The human connectome project: a data acquisition perspective," *Neuroimage* 62(4), 2222–2231 (2012). [PubMed: 22366334]
- [3]. Glasser MF, Sotiropoulos SN, Wilson JA, Coalson TS, Fischl B, Andersson JL, Xu J, Jbabdi S, Webster M, Polimeni JR, et al. , "The minimal preprocessing pipelines for the human connectome project," *Neuroimage* 80, 105–124 (2013). [PubMed: 23668970]
- [4]. Weninger L, Na C-H, Jutten K, and Merhof D, "Analyzing the effects of free water modeling by deep learning" on diffusion mri structural connectivity estimates in glioma patients," *PLoS One* 15(9), e0239475 (2020).
- [5]. Basser PJ, Mattiello J, and LeBihan D, "Mr diffusion tensor spectroscopy and imaging," *Biophysical journal* 66(1), 259–267 (1994). [PubMed: 8130344]
- [6]. Pasternak O, Sochen N, Gur Y, Intrator N, and Assaf Y, "Free water elimination and mapping from diffusion mri," *Magnetic Resonance in Medicine: An Official Journal of the International Society for Magnetic Resonance in Medicine* 62(3), 717–730 (2009).
- [7]. Hoy AR, Koay CG, Kecskemeti SR, and Alexander AL, "Optimization of a free water elimination two-compartment model for diffusion tensor imaging," *Neuroimage* 103, 323–333 (2014). [PubMed: 25271843]



- [8]. Molina-Romero M, Gómez PA, Albarqouni S, Sperl JI, Menzel MI, and Menze BH, “Deep learning with synthetic data for free water elimination in diffusion mri,” in [Proc Intl Soc Mag Reson Med], (2018).
- [9]. Arezza NJ, Santini T, Omer M, and Baron CA, “Estimation of free water-corrected microscopic fractional anisotropy,” *Frontiers in Neuroscience* 17, 1074730 (2023).
- [10]. Golub M, Neto Henriques R, and Gouveia Nunes R, “Free-water dti estimates from single b-value data might seem plausible but must be interpreted with care,” *Magnetic resonance in medicine* 85(5), 2537–2551 (2021). [PubMed: 33270935]
- [11]. Bergmann Ø, Henriques R, Westin C-F, and Pasternak O, “Fast and accurate initialization of the free-water imaging model parameters from multi-shell diffusion mri,” *NMR in Biomedicine* 33(3), e4219 (2020).
- [12]. Hoy AR, *Diffusion Tensor Imaging with Free Water Elimination*, PhD thesis, The University of Wisconsin-Madison (2015).
- [13]. Lee JM, [Introduction to Riemannian manifolds], vol. 2, Springer (2018).
- [14]. Yao T, Newlin N, Kanakaraj P, Cai LY, Ramadass K, Schilling K, Landman BA, Huo Y, et al., “A unified single-stage learning model for estimating fiber orientation distribution functions on heterogeneous multi-shell diffusion-weighted mri,” arXiv preprint arXiv:2303.16376 (2023).
- [15]. Van Essen DC, Smith SM, Barch DM, Behrens TE, Yacoub E, Ugurbil K, Consortium W-MH, et al. , “The wu-minn human connectome project: an overview,” *Neuroimage* 80, 62–79 (2013). [PubMed: 23684880]
- [16]. Scherrer B. and Warfield SK, “Why multiple b-values are required for multi-tensor models. evaluation with a constrained log-euclidean model,” in [2010 IEEE International Symposium on Biomedical Imaging: From Nano to Macro], 1389–1392, IEEE (2010).
- [17]. Molina-Romero M, Wiestler B, Gómez PA, Menzel MI, and Menze BH, “Deep learning with synthetic diffusion mri data for free-water elimination in glioblastoma cases,” in [International Conference on Medical Image Computing and Computer-Assisted Intervention], 98–106, Springer (2018).
- [18]. Goodwin-Allcock T, McEwen J, Gray R, Nachev P, and Zhang H, “How can spherical cnns benefit ml-based diffusion mri parameter estimation?,” in [Computational Diffusion MRI: 13th International Workshop, CDMRI 2022, Held in Conjunction with MICCAI 2022, Singapore, Singapore, September 22, 2022, Proceedings], 101–112, Springer (2022).
- [19]. Liu H, Fan Y, Li H, Wang J, Hu D, Cui C, Lee HH, Zhang H, and Oguz I, “Moddrop++: A dynamic filter network with intra-subject co-training for multiple sclerosis lesion segmentation with missing modalities,” in [International Conference on Medical Image Computing and Computer-Assisted Intervention], 444–453, Springer (2022).
- [20]. Cobb OJ, Wallis CG, Mavor-Parker AN, Marignier A, Price MA, d’Avezac M, and McEwen JD, “Efficient generalized spherical cnns,” arXiv preprint arXiv:2010.11661 (2020).
- [21]. Huo Y, Xu Z, Xiong Y, Aboud K, Parvathaneni P, Bao S, Bermudez C, Resnick SM, Cutting LE, and Landman BA, “3d whole brain segmentation using spatially localized atlas network tiles,” *NeuroImage* 194, 105–119 (2019). [PubMed: 30910724]
- [22]. Jenkinson M, Beckmann CF, Behrens TE, Woolrich MW, and Smith SM, “Fsl,” *Neuroimage* 62(2), 782–790 (2012). [PubMed: 21979382]
- [23]. Henriques RN, Rokem A, Garyfallidis E, St-Jean S, Peterson ET, and Correia MM, “[re] optimization of a free water elimination two-compartment model for diffusion tensor imaging,” *BioRxiv*, 108795 (2017).
- [24]. Ozarslan E, Koay C, Shepherd TM, Blackband SJ, and Basser PJ, “Simple harmonic oscillator based reconstruction and estimation for three-dimensional q-space mri,” in [Proc. Intl. Soc. Mag. Reson. Med], 17, 1396, Citeseer (2009).
- [25]. Nath V, Schilling KG, Parvathaneni P, Hansen CB, Hainline AE, Huo Y, Blaber JA, Lyu I, Janve V, Gao Y, et al. , “Deep learning reveals untapped information for local white-matter fiber reconstruction in diffusion-weighted mri,” *Magnetic resonance imaging* 62, 220–227 (2019). [PubMed: 31323317]

- [26]. Cheng J, Jiang T, and Deriche R, "Theoretical analysis and practical insights on eap estimation via a unified hardi framework," in [MICCAI Workshop on Computational Diffusion MRI (CDMRI)], (2011).

Author Manuscript

Author Manuscript

Author Manuscript

Author Manuscript



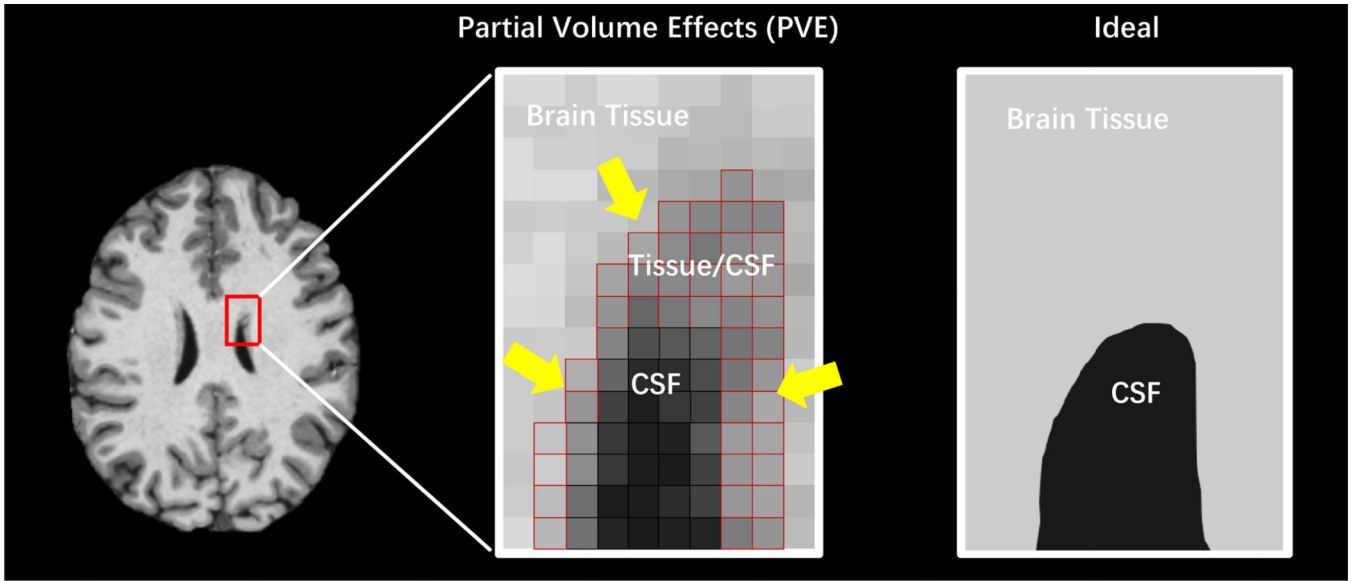


**Figure 1:**

The Free Water partial volume effects manifest at the boundary between brain tissue and ventricles filled with cerebrospinal fluid (CSF). The image to the right presents a pristine slice where the distinction between the brain tissue and CSF is sharp and clear. In contrast, the central image reveals partial volume effects in voxels encompassing both CSF and tissue, as indicated by the yellow arrows. The primary objective of the proposed algorithm is to extract parameter estimates that are exclusive to the tissue within these voxels.

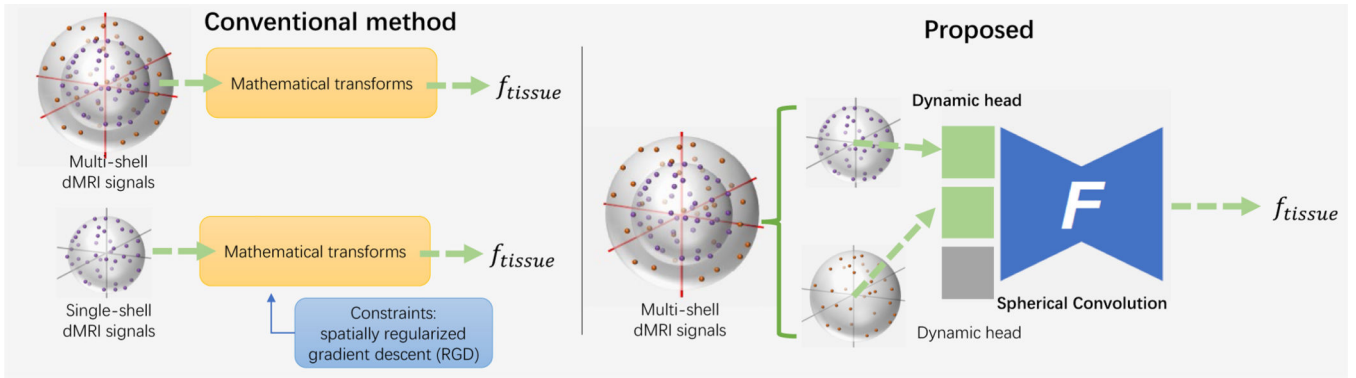


**Figure 2:**

Conventional methods have imposed constraints via the time evolution of a gradient flow on a Riemannian manifold to get a unique solution for the free water elimination on single-shell dMRI. Previous deep learning approaches achieve accurate model fitting for multi-shell and single-shell data. However, this framework did not allow for variations in input data size and therefore did not achieve a unified model for both data types. The prediction result shall have a significant bias when fed with dMRI from an unseen acquisition scheme. In our study, we proposed a single holistic model for different shell configurations that can recover/predict microstructural measures. Both single-shell and multi-shell dMRI sequences can be fed into the model together to improve the model performance on various shell configurations.

### Fractional Anisotropy Histogram

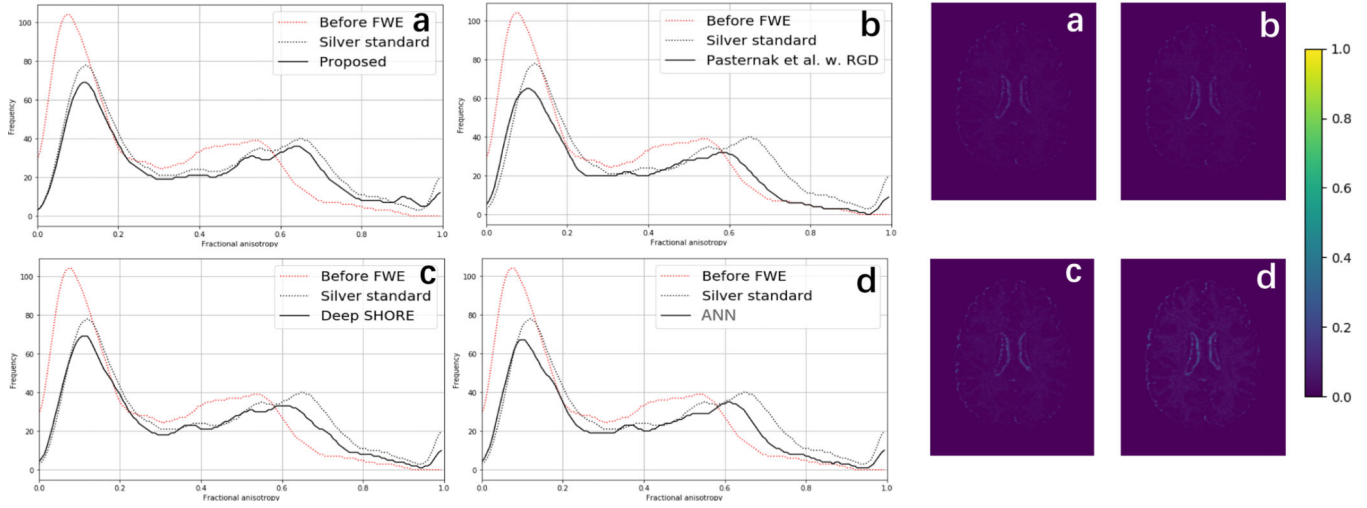


**Figure 3:** The histogram of the FA is shown before and after FWE from different methods respectively in the left panel. To further assess the transform/prediction, the FA error map with the silver standard is depicted in the right panel.

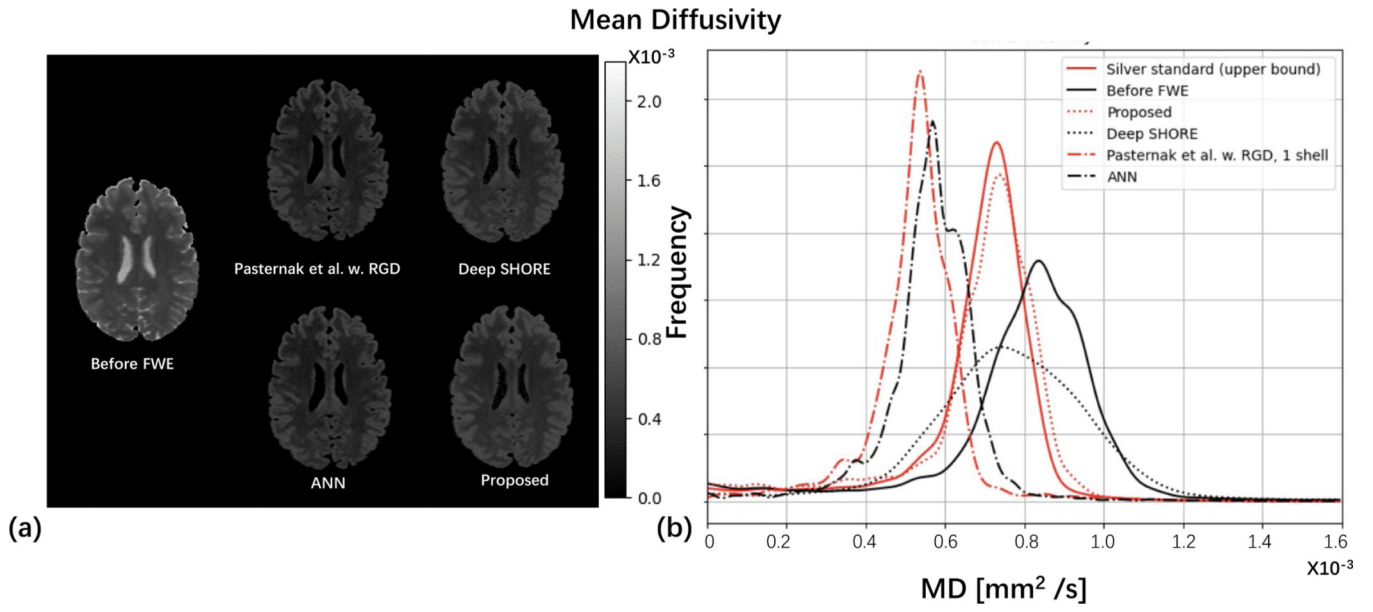


**Figure 4:**  
 The mean diffusivity of before/after different Free Water correction methods is qualitatively depicted in (a). To further assess the correction effect, the histogram of MD is shown in (b).

**Table 1:**

Comparison of metrics between methods. Both Deep SHORE and our proposed method are trained on a variety of shell configurations to improve the capability of the model. ANN is trained only with single-shell dMRI. The RMSE of  $f_{tissue}$  is applied to test the precision of different methods. The FA of ROI patches is to assess the correction effects of different methods. A statistical test was conducted, resulting in a significant difference with  $p < 0.001$

	Method	Metrics	
		RMSE of $f_{tissue}$	FA (ROI)
Before FWE			0.453
Conventional method	Pasternak et al. <sup>6</sup> w. RGD <sup>13</sup>	3.62E-02	0.498
Deep-learning based method	ANN <sup>8,17</sup>	3.08E-02	0.493
	Deep SHORE <sup>25</sup>	2.89E-02	0.501
	Proposed	<b>1.97E-02</b>	<b>0.508</b>
Silver standard (upper bound)			0.517